Target And Background Separation in Hyperspectral Imagery for Automatic Target Detection

Ahmad W. Bitar[1] & Loong-Fah Cheong[2] & Jean-Philippe Ovarlez[1,3]

[1]SONDRA/CentraleSupélec, Plateau du Moulon, 3 rue Joliot-Curie, F-91190 Gif-sur-Yvette, France
[2]National University of Singapore (NUS), Singapore, Singapore
[3]ONERA, DEMR/TSI, Chemin de la Hunière, 91120 Palaiseau, France

CentraleSupélec

Abstract
Based on a modification of the Robust Principal Component Analysis (RPCA), we regard the given hyperspectral image (HSI) as being made up of the sum of low-rank background HSI and a sparse target HSI that contains the targets based on a pre-learned target dictionary specified by the user. The proposed method is evaluated on both synthetic and real experiments.

What is a hyperspectral image (HSI)?
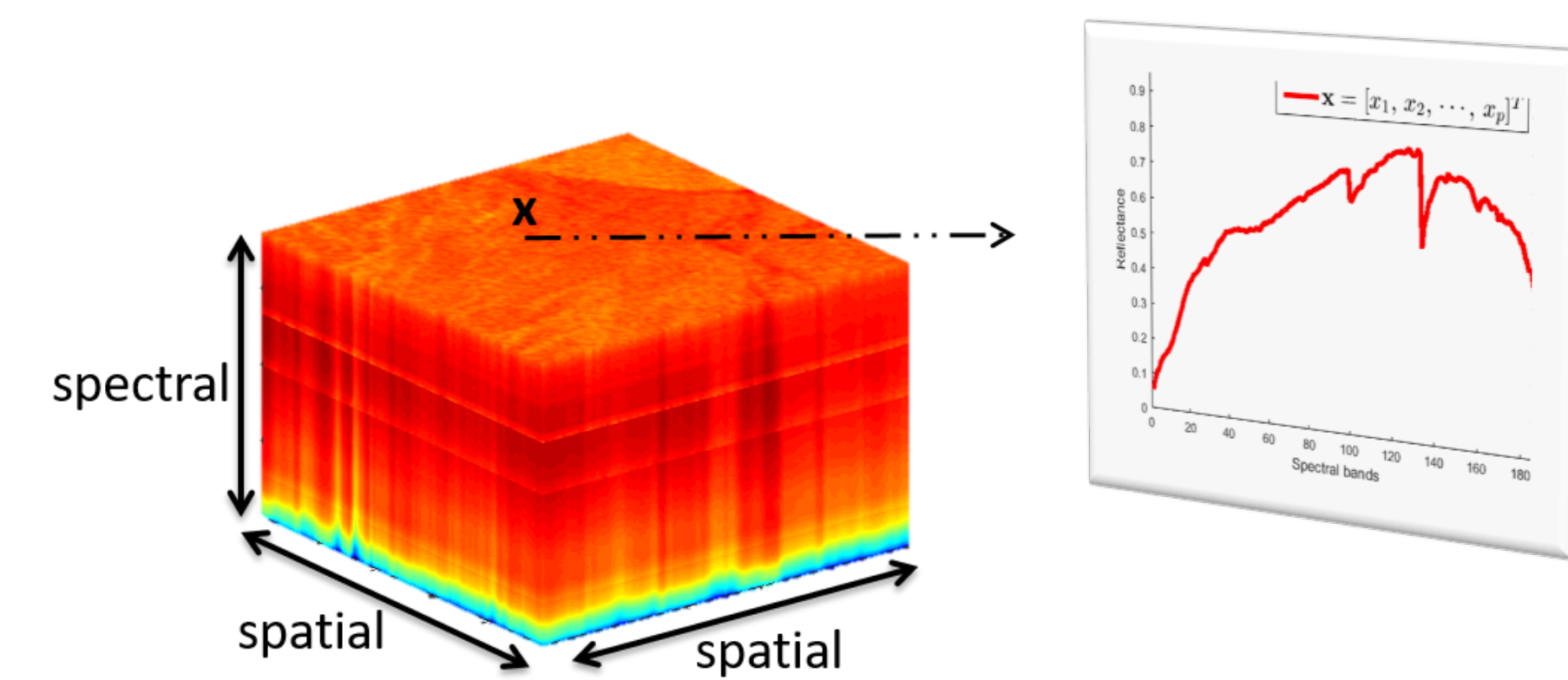
Figure 1.: A hyperspectral image (HSI)

A hyperspectral image (HSI) is a three dimensional data cube consisting of a series of images of the same spatial scene in a contiguous and multiple narrow spectral wavelength (color) bands.

Each pixel in the HSI is a p-dimensional vector, $\mathbf{x} \in \mathbb{R}^p$, where p stands for the total number of spectral bands.

Hyperspectral target detection

With the rich information afforded by the high spectral dimensionality, target detection is not surprisingly one of the most important applications in hyperspectral imagery.

Usually, the detection is built using a binary hypothesis test:

1. Null hypothesis (H_0)   The test pixel $\mathbf{x}$ consists only of background,

2. Alternative hypothesis (H_1)   The test pixel $\mathbf{x}$ may be either fully or partially occupied by the target material.

We can regard each test pixel as being made up of:

$$\mathbf{x} = \alpha\,\mathbf{t} + (1-\alpha)\,\mathbf{b}, \quad 0 \leq \alpha \leq 1$$

where:

- α: designates the target fill-fraction,
- $\mathbf{t}$: is the spectrum of the target,
- $\mathbf{b}$: is the spectrum of the background.

In case when $\alpha = 1$, the pixel $\mathbf{x}$ is fully occupied by the target material and is usually referred as full or resolved target pixel. When $0 < \alpha < 1$, the pixel $\mathbf{x}$ is partially occupied by the target material, and is usually referred as subpixel or unresolved target.

Our study on exploiting RPCA for hyperspectral target detection

How is RPCA exploited?

Based on similar assumptions as to those used in Robust Principal Component Analysis (RPCA):

1. the background is not too heavily cluttered with many materials with multiple spectra, so that the background signals should span a low-dimensional subspace, a property that can be expressed as the low rank condition of a suitably formulated matrix,

2. the total image area of all the target(s) should be small relative to the whole image (i.e. spatially sparse), e.g., several hundred pixels in a million pixel image, though there is no restriction on target shape or the proximity between targets.
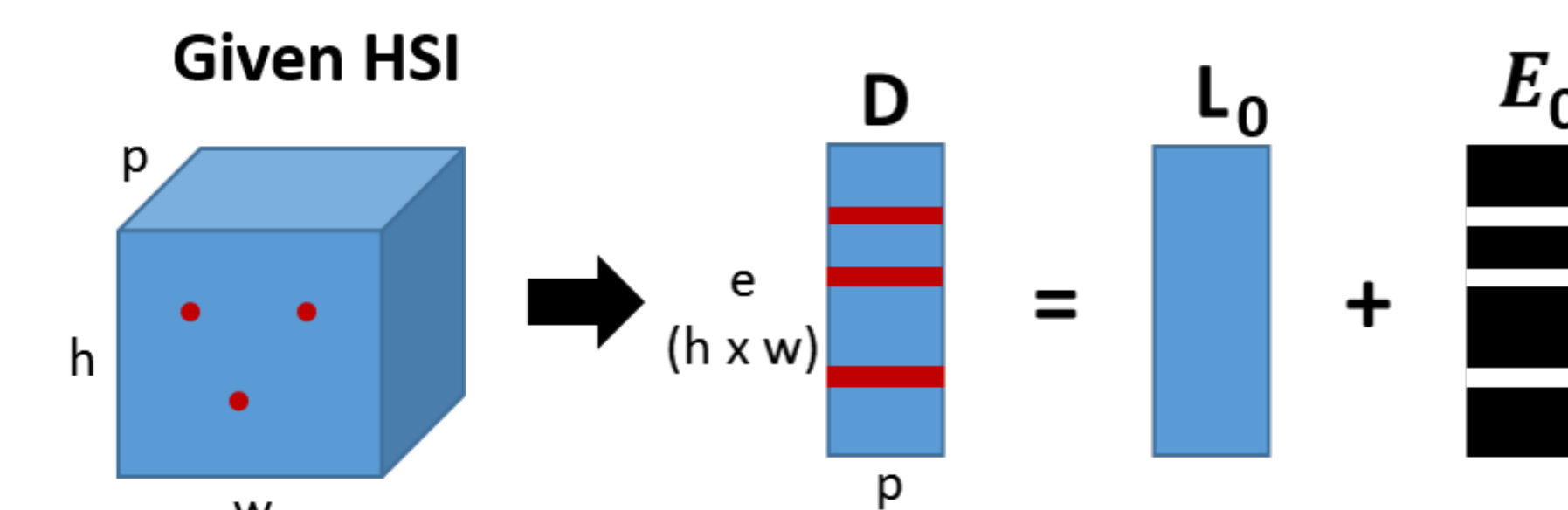
Figure 2.: A given HSI that contains three targets (the red circles). The HSI is split into a low rank background HSI $\mathbf{L}_0$, plus a sparse target HSI $\mathbf{E}_0$.

To estimate both $\mathbf{L}_0$ and $\mathbf{E}_0$, the RPCA considers the following minimization problem:

$$\min_{\mathbf{L},\mathbf{E}} \left\{ \mathrm{rank}(\mathbf{L}) + \lambda\,\|\mathbf{E}\|_{0,2} \right\}$$
$$s.t. \quad \mathbf{D} = \mathbf{L} + \mathbf{E}, \quad (1)$$

where λ controls the sparsity level in $\mathbf{E}$.

Problem (1) is NP-HARD to solve due to the $\mathrm{rank}(.)$ term and $l_{0,2}$ norm. Thus, it is solved by the following convex minimization problem (after surrogating the rank term by the nuclear norm and the $l_{0,2}$ norm by the $l_{1,2}$ norm):

$$\min_{\mathbf{L},\mathbf{E}} \left\{ \tau\,\|\mathbf{L}\|_* + \lambda\,\|\mathbf{E}\|_{1,2} + \|\mathbf{D} - \mathbf{L} - \mathbf{E}\|_F^2 \right\}, \quad (2)$$

where τ controls the rank of $\mathbf{L}$, and λ the sparsity level in $\mathbf{E}$.

Is RPCA adequate to identifying the true targets?

No!

The following evaluations prove that the direct use of RPCA:

1. is inadequate to distinguishing the true targets from the background.

2. searches only for small heterogeneous and/or high contrast regions!

Evaluation on the DATA HSI (of size $201 \times 200 \times 167$)
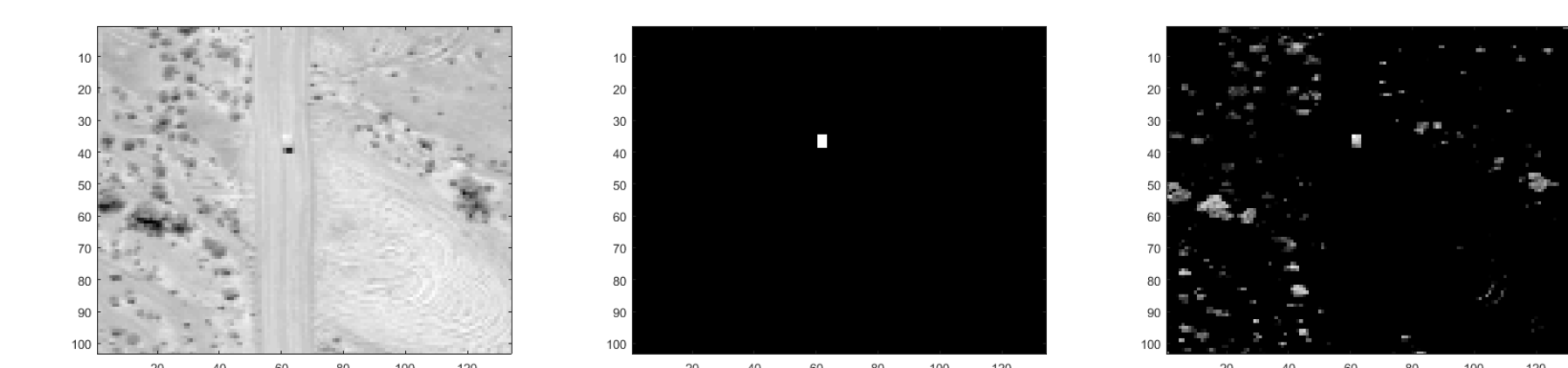
Figure 3.: From left to right: the original HSI (mean power in dB over the 167 spectral bands) the ground truth image for the targets of interests; the sparse target HSI $\mathbf{E}$ after some thresholding (mean power in dB).

Evaluation on the Cuprite HSI (of size $250 \times 291 \times 186$)
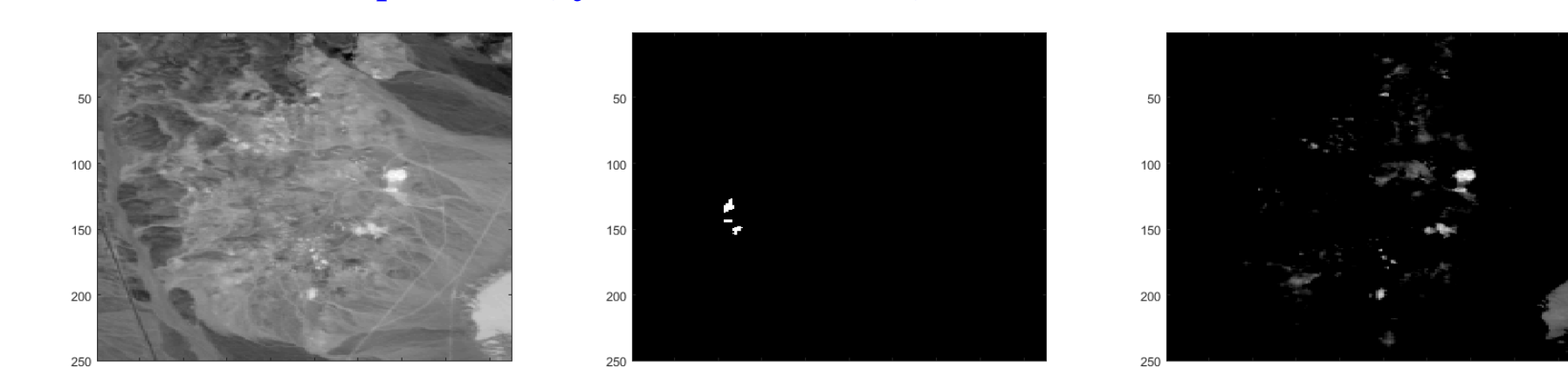
Figure 4.: From left to right: the original HSI (mean power in dB over the 186 spectral bands); the ground truth image for the targets of interests; the sparse target HSI $\mathbf{E}$ after some thresholding (mean power in dB).

Our modification of RPCA

We consider that a prior target information is provided to the user. This prior information is related to the target spectra.

In this regard, we use a pre-learned target dictionary $\mathbf{A}_t$ to cast the general RPCA into a more specific form, specifically, we further factorize the sparse component $\mathbf{E}$ from RPCA into the product of $\mathbf{A}_t$ and a sparse activation matrix $\mathbf{C}$:

$$\mathbf{D} = \mathbf{L}_0 + (\mathbf{A}_t\,\mathbf{C}_0)^T + \mathbf{N}_0,$$

where

- $(\mathbf{A}_t \mathbf{C}_0)^T$ is the sparse target matrix.

- $\mathbf{A}_t$ is the target dictionary containing the target samples.

- The coefficient matrix $\mathbf{C}_0$ that should be sparse in columns.

- $\mathbf{N}_0$ is assumed to be independent and identically distributed Gaussian noise with zero mean and unknown standard deviation.

Both the low rank component ($\mathbf{L}_0$) and sparse component $(\mathbf{A}_t \mathbf{C}_0)^T$ are estimated as follows:

$$\min_{\mathbf{L},\mathbf{C}} \left\{ \tau\,\mathrm{rank}(\mathbf{L}) + \lambda\,\|\mathbf{C}\|_{2,0} + \|\mathbf{D} - \mathbf{L} - (\mathbf{A}_t\mathbf{C})^T\|_F^2 \right\}, \quad (3)$$

where τ controls the rank of $\mathbf{L}$, and λ the sparsity level in $\mathbf{C}$.

Problem (3) is surrogated towards the following convex minimization problem:

$$\min_{\mathbf{L},\mathbf{C}} \left\{ \tau\,\|\mathbf{L}\|_* + \lambda\,\|\mathbf{C}\|_{2,1} + \|\mathbf{D} - \mathbf{L} - (\mathbf{A}_t\mathbf{C})^T\|_F^2 \right\}, \quad (4)$$

Synthetic experiments

The experiments are done on a $101 \times 101 \times 186$ HSI zone (see Figure 5).

1. We incorporate in this zone, 7 target blocks (each of size 6×3) with $\alpha \in [0.01, 1]$ (all have the same α), placed in long convoy formation all formed by the same synthetic (perfect) target $\mathbf{t}$ consisting of a sulfate mineral type known as "Jarosite".

2. The target $\mathbf{t}$ that we created actually consists of the mean of the first six Jarosite mineral samples taken from the USGS Spectral Library.

3. As for $\mathbf{A}_t$, it is constructed from the six acquired Jarosite samples (see Figure 5).
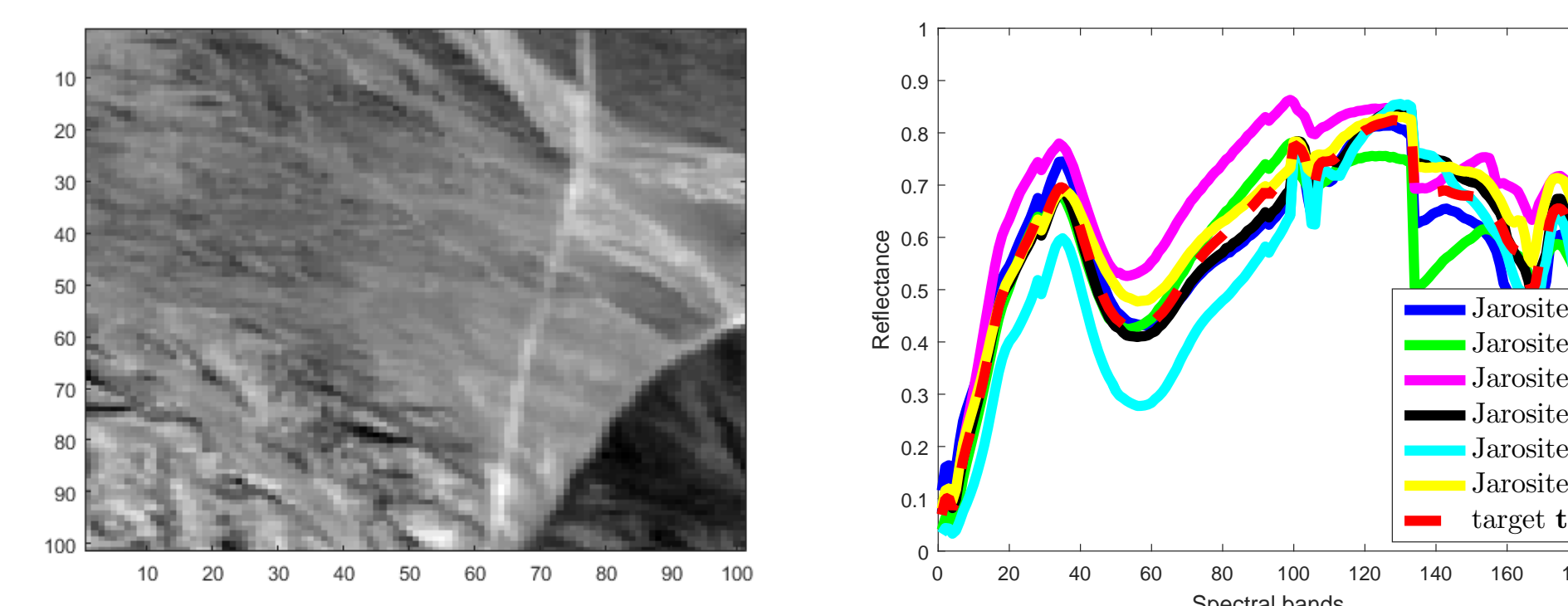
Figure 5.: From left to right: the $101 \times 101 \times 186$ HSI zone (we exhibit the mean power in dB over the 186 spectral bands); Plot of the Jarosite samples taken from the online USGS Spectral library.

Visual target detections of $(\mathbf{A}_t\mathbf{C})^T$:

Figure 6 depicts a 2-D visual detection results of $(\mathbf{A}_t\mathbf{C})^T$ for different α values. Obviously, all the targets are detected with little false alarms until $\alpha \leq 0.1$ when a lot of false alarms appear.
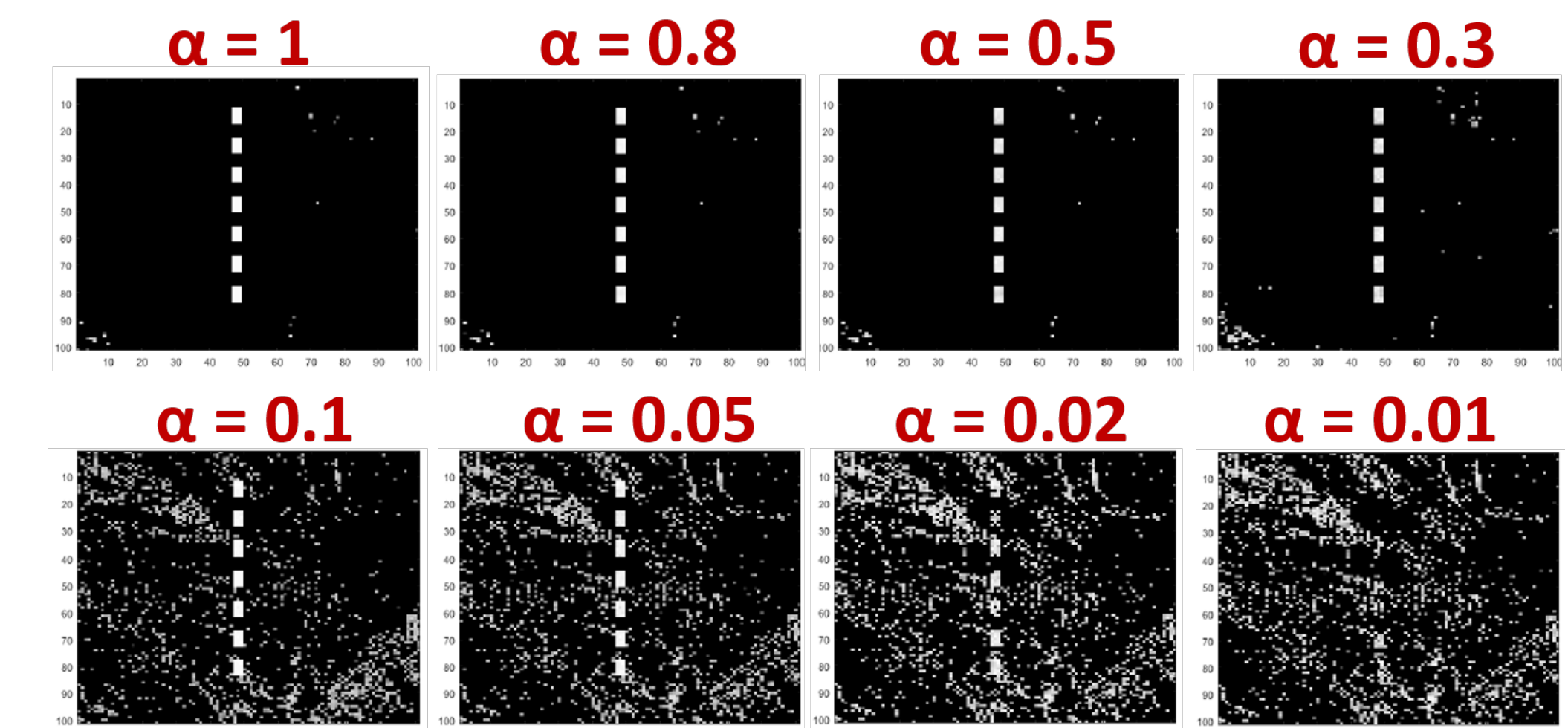
Figure 6.: Visual detections (mean power in dB over the 186 bands) of $(\mathbf{A}_t\mathbf{C})^T$ for the 7 target blocks for different α.

Real Experiments

1. The experiments are based on a HSI zone of size $250 \times 291 \times 186$ pixels (see Figure 7)

2. We consider this HSI zone specifically to detect the Tectosilicate mineral type target pixels known as Buddingtonite.

3. There are three Buddingtonite samples available in the online ASTER spectral library, and our target dictionary $\mathbf{A}_t$ is formed by these samples (see Figure 7).
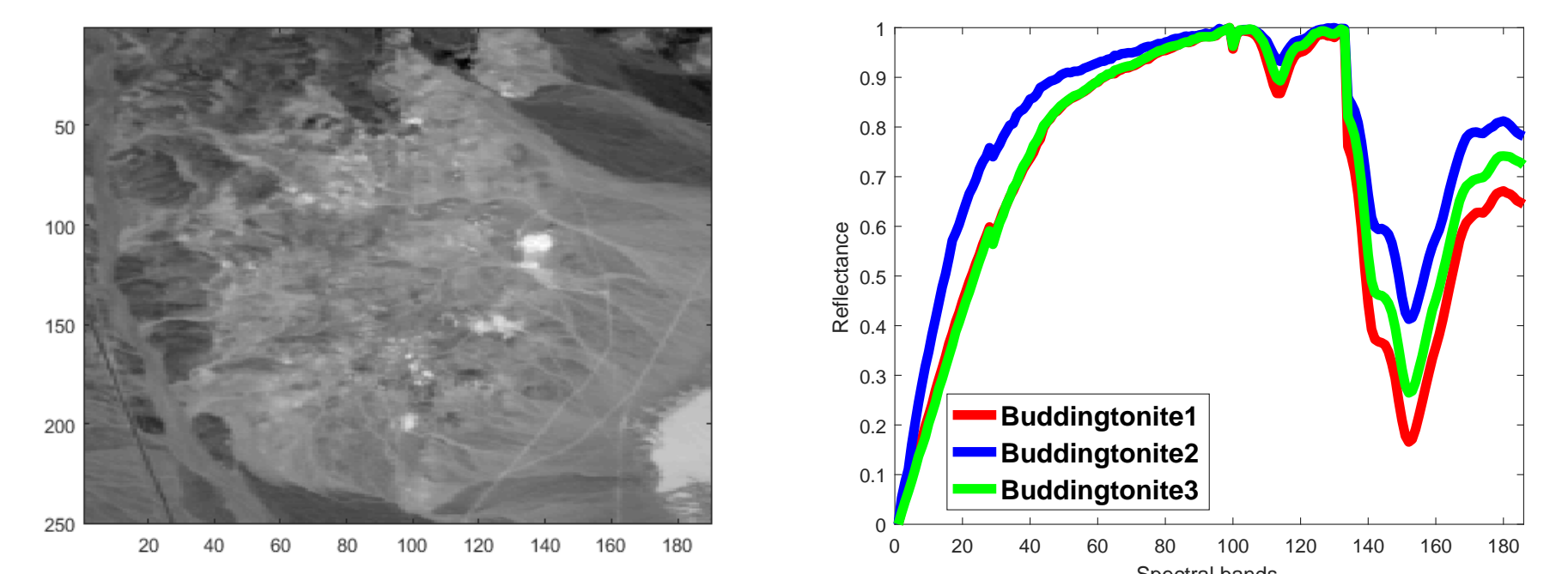
Figure 7.: From left to right: the $250 \times 291 \times 186$ HSI zone (mean power in dB over the 186 spectral bands); Plot of the Buddingtonite target samples taken from the online ASTER Spectral library.

Visual target detections of $(\mathbf{A}_t\mathbf{C})^T$:

Figure 8 depicts the visual detection of the Buddingtonite targets in $(\mathbf{A}_t\mathbf{C})^T$. The Buddingtonite targets are detected with very little false alarms.
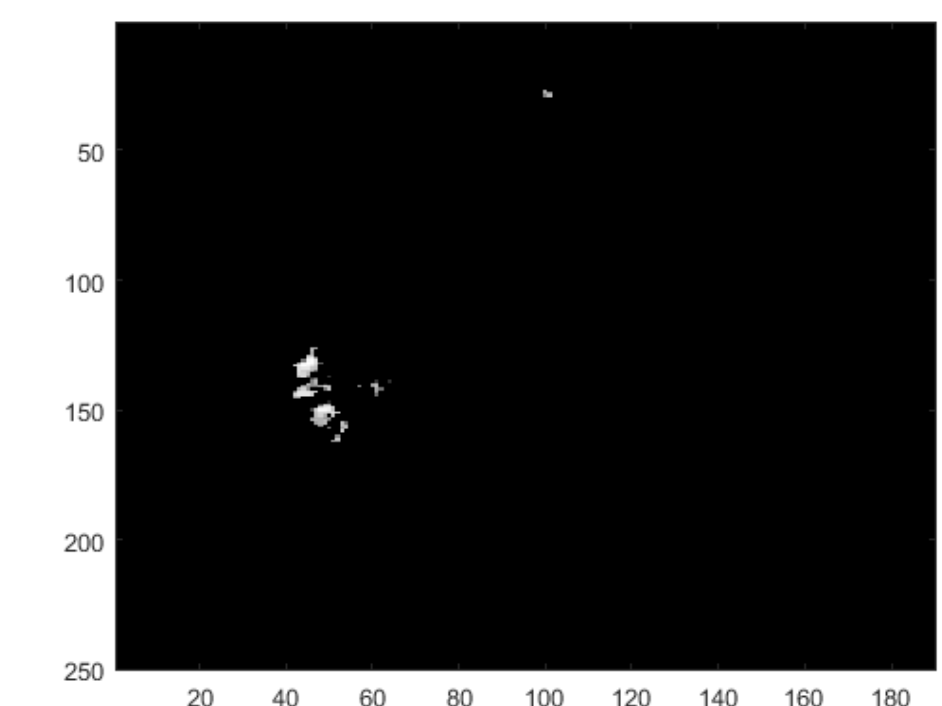
Figure 8.: The detection in $(\mathbf{A}_t\mathbf{C})^T$ (mean power in dB over the 186 bands).

Concluding remarks

- The obtained results demonstrate the effectiveness of our modified RPCA for hyperspectral target detection. In particular, they can deal with targets of any shapes or targets that occur in close proximity, and are resilient to most values of fill-fractions unless they are too small!!

- The subspace overlap problem illustrated in Figure 4 is now much relieved, as can be seen from Figure 8 ☺☺☺